Computers & Geosciences 105 (2017) 103–112

Contents lists available at ScienceDirect

Computers & Geosciences

journal homepage: www.elsevier.com/locate/cageo

Research paper

A geophone wireless sensor network for investigating glacier stick-slip motion

Kirk Martinez[a,*], Jane K. Hart[b], Philip J. Basford[a], Graeme M. Bragg[a], Tyler Ward[a], David S. Young[a]

[a] Electronics and Computer Science, University of Southampton, Southampton SO17 1BJ, UK
[b] Geography and Environment, University of Southampton, Southampton SO17 1BJ, UK

ARTICLE INFO

Keywords:
Environmental sensor network
Geophones
Glacier velocity

ABSTRACT

We have developed an innovative passive borehole geophone system, as part of a wireless environmental sensor network to investigate glacier stick-slip motion. The new geophone nodes use an ARM Cortex-M3 processor with a low power design capable of running on battery power while embedded in the ice. Only data from seismic events was stored, held temporarily on a micro-SD card until they were retrieved by systems on the glacier surface which are connected to the internet. The sampling rates, detection and filtering levels were determined from a field trial using a standard commercial passive seismic system. The new system was installed on the Skalafellsjökull glacier in Iceland and provided encouraging results. The results showed that there was a relationship between surface melt water production and seismic event (ice quakes), and these occurred on a pattern related to the glacier surface melt-water controlled velocity changes (stick-slip motion). Three types of seismic events were identified, which were interpreted to reflect a pattern of till deformation (Type A), basal sliding (Type B) and hydraulic transience (Type C) associated with stick-slip motion.

1. Introduction

The motion of glaciers is highly dependent on the behaviour of meltwater (generated at the glacier surface by atmospheric melting) which can influence the rate at which glaciers move by creep (Duval, 1977), reduce friction to allow basal sliding (Weertman, 1957; Iken et al., 1983), and deform underlying sediments (Boulton and Jones, 1979). Recent studies of continuous measurements of glacier velocities by GPS have indicated that ice motion is commonly episodic and it has been proposed that this reflects stick-slip motion (Bahr and Rundle, 1996; Fischer and Clarke, 1997; Tsai and Ekstrom, 2007; Wiens et al., 2008). Such a process would generate microseismic events (ice quakes) at the glacier bed, which could be measured by seismometers (Weaver and Malone, 1979; Anandakrishnan and Bentley, 1993; Metaxian et al., 2003; Smith, 2006). However, other sources of ice quakes within the glacial environment include ice calving (Qamar, 1988; O'Neel and Pfeffer, 2007), crevassing (Neave and Savage, 1970; Deichmann et al., 2000) and basal fracture (Walter et al., 2008).

Wireless sensor networks which are designed to be deployed for earth-science research have brought low power networking to remote areas (Chong and Kumar, 2003; Martinez et al., 2004; Hart and Martinez, 2006; Gehrke and Liu, 2006; Oliveira and Rodrigues, 2011; Huang et al., 2015). These environmental sensor networks have enabled a wider range of areas to be monitored for fundamental science and hazard warnings (Szewczyk et al., 2004; Delin et al., 2005; Werner-Allen et al., 2005; Hasler et al., 2008; Xu et al., 2014).

Most current commercial passive seismic systems require large power supplies and do not provide "live" data. Surface based deployments also require regular manual re-levelling, due to surface melt. In contrast, we required a long-term, low power automatic system housed in a borehole in order to avoid re-levelling, lessen the effects of noise from the glacier surface and insure a direct contact with the ice. We have developed a low power borehole geophone as part of a wireless sensor network, which can be used alongside GPS, subglacial wireless probes (Martinez et al., 2004), temperature and time lapse camera data (Young et al., 2015) to monitor a range of glacial processes. One advantage of the sensor network is its ability to send data back to a server in the UK daily, which provides researchers with a "live" feed via an internet connection. Due to the potentially high levels of data produced from continuous recording, we used an event detection system, so that the system only stored and communicated data related to the ice quakes (events). This new system, which is the first of its kind, consists of a small, borehole based, low power, event detection system providing a "live" data stream. The design has the potential to

* Corresponding author.
E-mail address: km@ecs.soton.ac.uk (K. Martinez).

http://dx.doi.org/10.1016/j.cageo.2017.05.005
Received 15 March 2016; Received in revised form 1 April 2017; Accepted 8 May 2017
Available online 10 May 2017

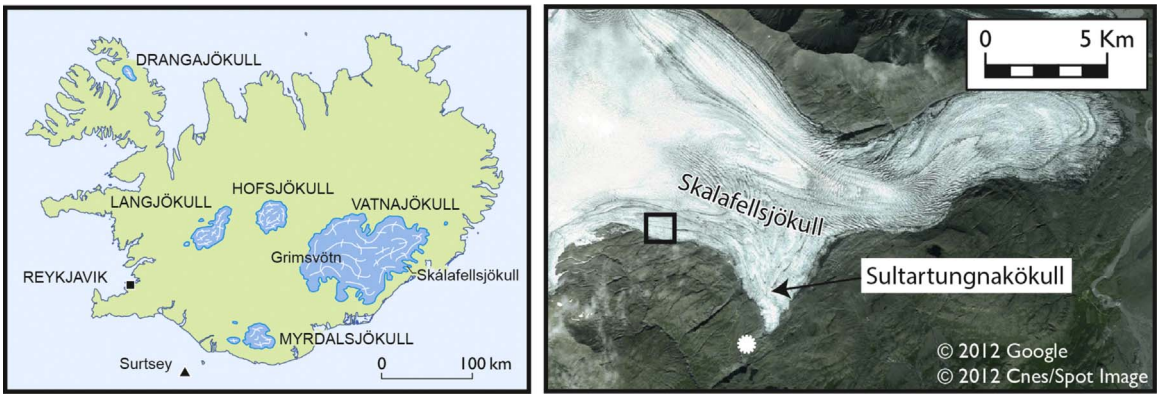

Fig. 1. Location of study area at Skálafellsjökull, b) Image of study area, square indicates main Glacsweb study site, star indicates camera location.

allow geophone sensing over longer time periods while providing researchers with frequent updates and an understanding of the state of the hardware. It could be used in other seismic deployments where long-term monitoring of short-term events is required.

The aims of this paper are:

- To discuss the design and development of the geophone system and its integration into a heterogeneous environmental sensor network.
- To report the findings from a field trial using a commercial passive seismic recording device on the glacier surface. This was undertaken to detect basal ice quakes and also investigate the required sampling rates, detection and filtering for our custom system.
- To present analysis of data generated from the new system to study the timing and nature of microseismicity associated with daily stick-slip motion at an Icelandic glacier.

2. The field site

Skalafellsjökull, Iceland (Fig. 1a) is an outlet glacier of the Vatnajökull icecap which rests on Upper Tertiary grey basalts. This glacier has an area of approximately 100 km^2 and is 25 km in length (Sigurðsson, 1998). The study site was located on the glacier at an elevation of 792 m a.s.l., where the ice was flat and crevasse free. The subglacial meltwater in this area emerged 3 km away at the southern part of the glacier (known as the Sultartungnajökull tongue, Fig. 1b).

The Glacsweb sensor network was deployed at Skalafellsjökull, Iceland (Fig. 1a) (2008–2013) and provided the ideal infrastructure for this research. This consisted of multiple heterogeneous nodes which have been developed during several years of continuous deployments (Martinez et al., 2009, 2012; Hart et al., 2006). Fig. 2 illustrates the design of the wireless sensor network system in 2012/3. A set of sensor nodes on/in the glacier used appropriate radio frequencies (868 MHz surface, 173 MHz ice) to communicate to a base station that uses either Wi-Fi or GPRS to send the data to a server hosted in the Amazon Web Services cloud (Martinez and Basford, 2011). As well as acting as routing nodes the gateways include a meteorological station, GPS, cameras and other diagnostic sensors. There were also four standalone dGPS units recording ice velocity 2012/3 and a time-lapse camera monitoring river discharge (Young et al., 2015).

Ground penetrating radar (GPR) surveys and borehole measurements have shown that the glacier at the study site ranges from 0 to 200 m in thickness. The glacier rests on a fine grained till, with a series of active till thrust sheets approximately 5 m thick, moving at 3 m per year throughout the year. The water content (calculated from GPR) of the glacier is very low (0.5%), but surface meltwater moves rapidly though englacial crevasses and moulins to the glacier bed (Hart et al., 2015). Data from the wireless Glacsweb probes show the water pressure in the till is high during the summer, but fluctuates during the winter depending on meltwater inputs.

Weather data were obtained from the base station and, during periods of mechanical failure, from a transfer function applied to data from the neighbouring Icelandic meteorological station at Höfn. Daily surface melt was calculated by the degree day algorithm (PDD) (Braithwaite, 1985; Hock, 2003), using degree day factors for Satujökull, Iceland (Johannesson et al., 1995), 5.6 mm d^{-1} $°C^{-1}$ for snow and 7.7 mm d^{-1} $°C^{-1}$ for ice. Albedo was calculated from the MODIS data, using the threshold between ice and snow to be 0.45, on a 30×30 m grid ASTER DEM.

3. Field trial using a commercial system in 2011

Six commercial geophones were installed on the glacier surface. Each station consisted of a 4.5 Hz 3-component geophone with pre-amplifier, powered by lead-acid battery and two 20 W solar panels. Data were recorded by ISSI (Integrated Seismic Systems International) SAQS (Stand Alone Quake Systems) systems units capable of sampling at up to 24 kHz. The units recorded 24 bit data per channel at a sample rate of 1 kHz. The systems were placed 90 m apart from so the spacing

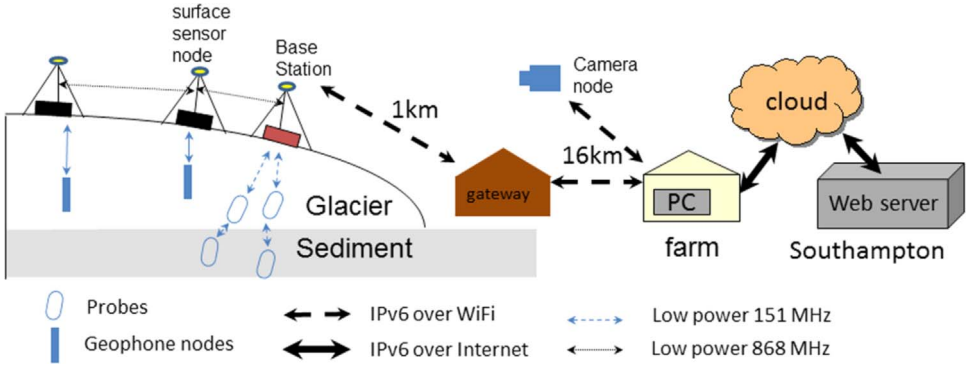

Fig. 2. Sensor network deployed in Iceland. Showing the geophone nodes integrated into the radio network.

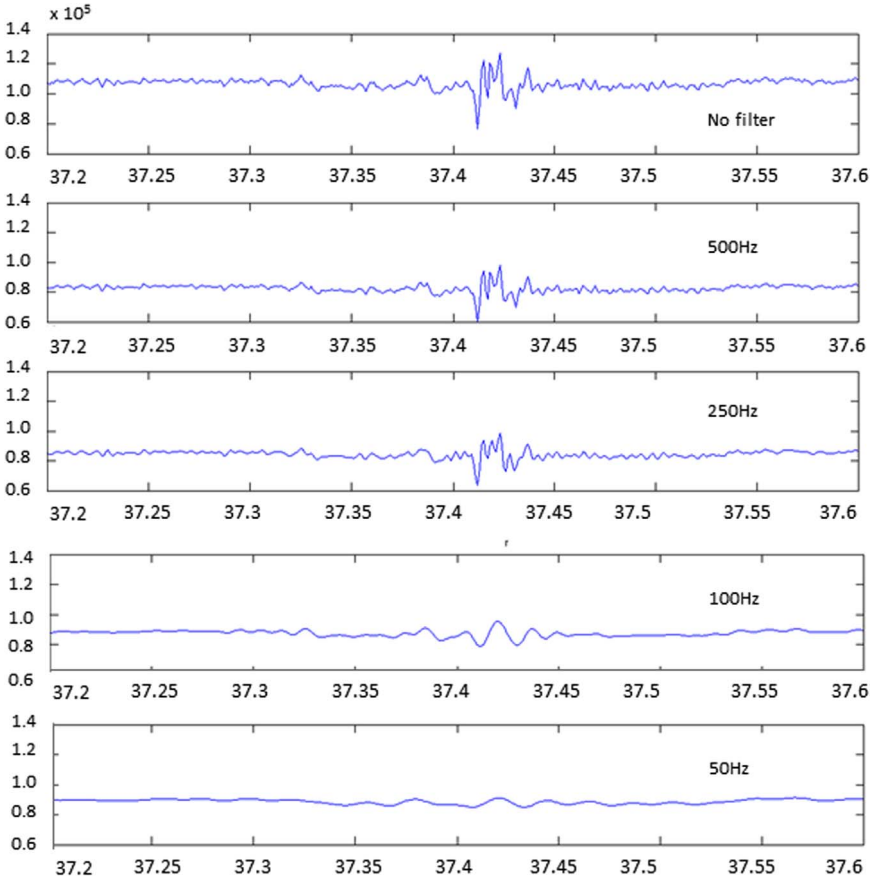

Fig. 3. Results of applying low pass filters to z component from the ISSI SAQS system.

between them was approximately equivalent to the ice thickness in the deployment region. The geophones were mounted on white plywood boards 0.5 m square which were dug down into the ice approximately 0.3 m and placed level and covered with ice chips. They required re-levelling and re-alignment with true north each day (Hart et al., 2011). Recording was carried out over 8 days, with some periods where one or two stations were not active but overall data was collected during 76% of the time available for the field trial.

Basal signals are typically marked by an initial P wave followed by the S wave. The approximate velocities of these waves in ice are well known (3600 m s^{-1}, 1800 m s^{-1}) (Röthlisberger, 1972), and the time difference between the arrivals can be used to calculate the ice quake source (Smith, 2006).

3.1. Sampling parameters and filtering

Our new geophone system required a sampling rate sufficient to capture the events (basal ice quakes) but not so high that it created unnecessary data volumes. Filtering can be used to separate the signal from the background in a data sample from the SAQS system. Fig. 3 shows the impact of low pass filtering at different frequencies (500, 250, 100 and 50 Hz) along with the unfiltered signal of the Z component of one of the units. The 500 and 250 Hz low pass filters still preserve the event, but it is reduced at 100 and 50 Hz. This shows that the new geophone nodes could use a sampling rate of 500 Hz with a low pass filter at 250 Hz (to satisfy the Nyquist criterion) without losing too much information. In order to detect an event in the SAQS system, we used a technique (Walter et al., 2008) which compares the root-mean-square (rms) values of a short term average (STA) and long term average (LTA). When the ratio STA/LTA is greater than a threshold an event is recorded. This threshold is adjusted through observation in order to pick out the P wave using SDX (Seismic Data eXplorer) software (http://doree.esc.liv.ac.uk:8080/sdx). It was found that a 10 Hz and 100 Hz band pass filter, with a threshold ratio around 10 and STA and LTA periods of 0.005 and 0.1 s respectively picks out the P wave reasonably well. The P wave pick times are generally located part way through the P wave up kick. Trials showed that lower thresholds and adjustments in the LTA/STA created more false events.

3.2. Basal events

Basal events are assumed to occur at ice depth or further from stations, and be detectable by several stations. There were at least 5 basal events that occurred on at least 4 stations. These occurred within the virtually continuous recording period from 17.00 h day of the year (DOY) 215–12.00 h DOY 219. Fig. 4 shows an example of the event 16:43:37 on DOY 218. The average difference in time between the P and S waves during this event was 0.03 s (s.d. 0.009), and for the five basal events 0.039 s (s.d. 0.014). The difference between the P and S waves gives an estimated distance of 72–205 m which is similar to depth recorded from the GPR survey (up to 200 m). This provides evidence that they were basal events.

Fig. 5 shows the air temperature, rainfall, recording time and seismic events during the fieldwork period. The seismic events occur during days of relatively high temperature (and low rainfall), over 8 °C, and very soon after peaks in temperature (9 min to 3 h 28 min). If these events represent stick-slip events then they show that the water melted from the glacier surface travels quickly to the base of the glacier where it lubricates the bed allowing it to rapidly slide.

3.3. Outcomes

The results of the 2011 field trial were to a) demonstrate that basal events occurred and could be detected by a passive seismic system; and

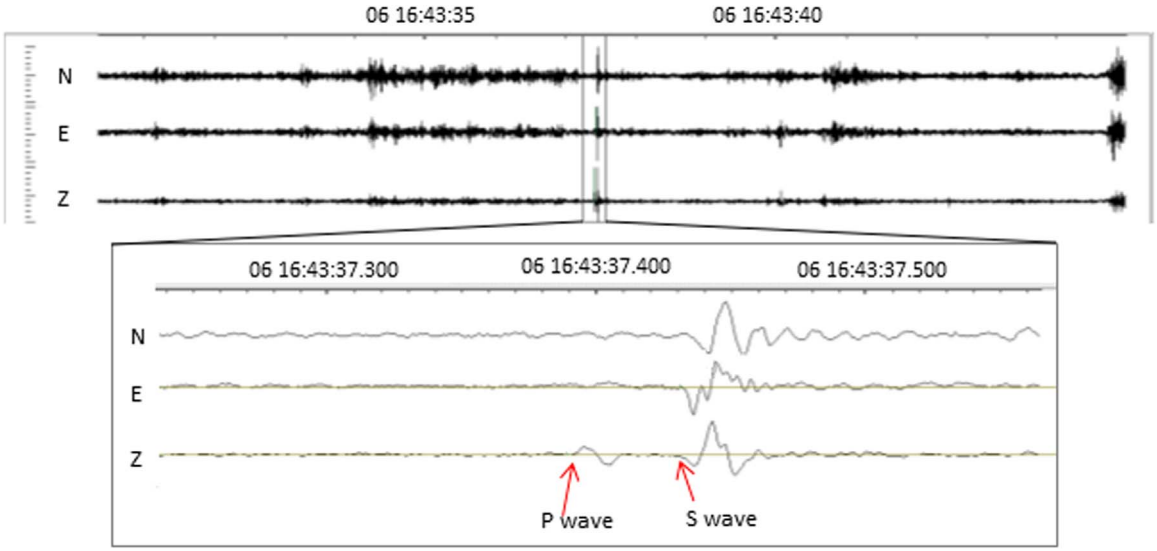

Fig. 4. Event 16:43:37 on DOY 218 SDX (Seismic data eXplorer).

b) to determine the appropriate parameters for the design of the Glacsweb geophones. A threshold ratio of 10, LTA of 0.1 s, STA of 0.005 s, a total record time of 1 s and pre-trigger record time of around 0.3 s was used as the basis for the design of the Glacsweb geophones.

4. Design of the geophone nodes

The geophone nodes were developed in 2012 as an integral part of the Glacsweb sensor network (Fig. 2). They consisted of a custom PCB using an ARM® Cortex®-M3 processor (Energy Micro EFM32G880F128), amplifiers and 2 GByte micro-SD card storage (Fig. 6). The 32-bit M3 processor, running at 28 MHz was powerful enough to carry out simple signal processing which may be required for the decision to store the data. The package included other desirable features including: 12-bit analogue to digital converters (ADC), six serial interfaces (UART) and very low power modes (0.9 μA sleep). The nodes were linked via an RS485 cable link directly to a seismic surface node (SSN) which stored and relayed the data. These surface nodes were used partly because of the relatively large volumes of data but also so that the geophone nodes could eventually use a short range radio link to them on the surface. They SSNs were based on a similar design with a micro-SD card for storing the data, so that in the event of the ice nodes being destroyed the data would be preserved. The serial cabled link is also more energy efficient than radio due to its relatively high data rate and low error rate.

As a borehole has to be drilled to insert the geophone node it was also simple to position a surface node above it and avoid surface runs of cable to the central base station. The cable link also allowed power to be sent to the geophone node from the SSN which has a larger 12AH battery. However, the cable is likely to break in a long deployment so the design also included a backup 173 MHz radio link. This frequency had been found to work well in glaciers (Hart et al., 2015) although it was not deployed due to a lack of testing. Data retrieved by on the surface node is then transferred via the 868 MHz radio network to the base station. This surface network was a custom design based on the Glacsweb packet structure used in the sub-glacial sensor nodes. A file

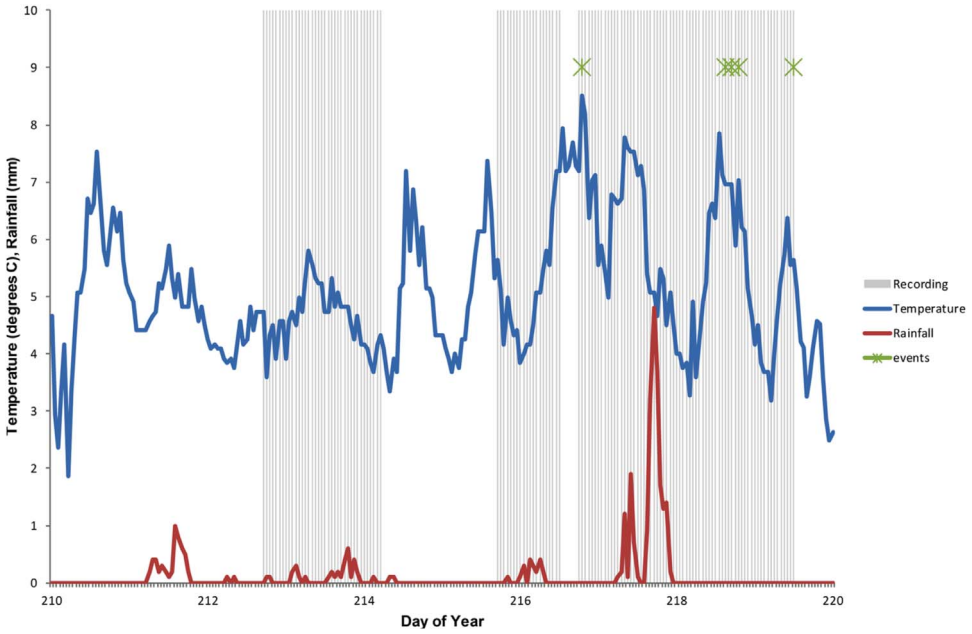

Fig. 5. Air temperature, rainfall, basal seismic events (green stars) when 3 or more stations were recording (grey) during the 2011 field trial. (For interpretation of the references to color in this figure legend, the reader is referred to the web version of this article.)

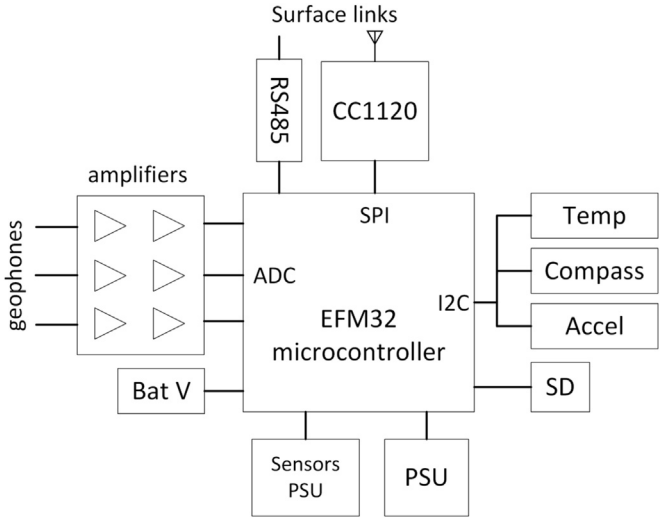

Fig. 6. Schematic of the geophone node electronics.

transfer protocol based on XMODEM was added in order to retrieve the files over radio links without any errors. The system was designed so that the data reaches a safer place with each transfer, from the node to the surface, to the base station then the server. This could give researchers new data every day as long as the surface networks were intact.

The geophone nodes continually sample the output of three orthogonal geophones and store the data to microSD only when an event is detected. We used 28 Hz Geospace GS-20DH geophones encapsulated in resin inside a 70 mm diameter polycarbonate tube

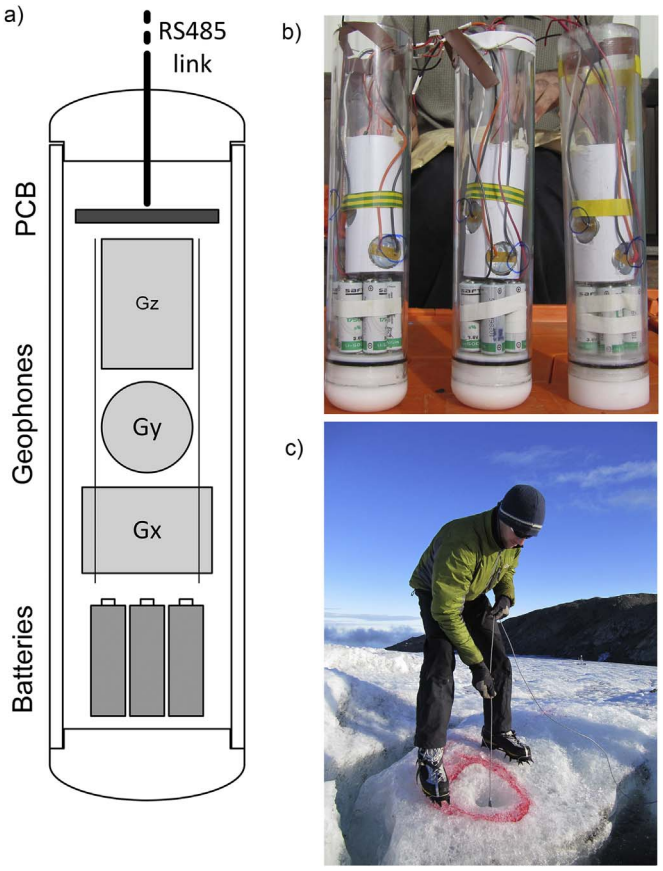

Fig. 7. Glacsweb low power geophone: a) diagram showing the component layout, b) photograph of nodes before potting, c) deploying a geophone node.

(Fig. 7a and b). These geophones were chosen because they had been used successfully in glacier borehole experiments with a commercial logger on the surface (Walter et al., 2008). Our nodes also measure their orientation, with a 3D accelerometer, digital compass and temperature. The nodes contained seven 14.5 AH 3.6 V Lithium Thionyl Chloride AA-size batteries for use when the surface power feed was unavailable. Fig. 7c shows one being lowered into a bore-hole.

The sampling parameters were chosen taking into account the experience with the commercial system. An instrumentation amplifier (INA321E) was used with a gain of 25 dB amplifier to provide sufficient signal. Then a bandpass filter of 0.5–234 Hz. The sampling rate of 512 Hz was chosen to preserve signals up to 256 Hz. The 12 bit ADCs where oversampled to provide 16 bits per sample.

In order to detect events the geophones have to be continuously sampled. However, continuous data storage from three sensors per node would lead to storage and transmission problems while providing little useful signal. To preserve battery life and avoid storing unwanted data a low power technique was devised. Continuous analogue to digital conversion was used, with the data being written to RAM using Direct Memory Access from the ADC while the rest of the hardware is in sleep mode. If the ADC comparator circuit detects an impulse in the signal it sets a flag which causes the processor to write the data buffer to the SD card (Martinez et al., 2012) when it is woken up. This was the simplest technique to implement for this prototype, however a filter-based algorithm (Song et al., 2009) could be implemented in hardware in the future to reduce noise sensitivity. If the node detected an event in the one second sample it recorded the data to a file on the micro-SD card. The binary file format created used a 28 byte header (time stamps) and each of the three channels in 16 bit words, for a total of 3100 bytes. The micro-SD card had a capacity of 2 GBytes and could therefore store 692,000 samples/events, which was far more than expected in one year. The surface nodes also have a 2 GByte card to store all data, which provides a backup which can be retrieved if the radio systems fail. The node uses 300 μA while sampling, with bursts of 3 mA when writing to the SD card.

5. Results from the WSN Geophones 2012

Four geophone nodes were installed within boreholes, to avoid surface seismic noise. Boreholes were drilled in the glacier with a Kärcher HDS1000DE jet wash system. The boreholes were located on a diamond grid, separated by the depth of the glacier. The nodes sat in the base of the 30 m deep boreholes which became embedded into the ice by freezing and creep. Due to the prototype nature of the enclosures and electronics only one geophone (ID 62) functioned for more than one day. It is possible that the cables and sealing failed in many of the nodes, which are too deep to recover once they are embedded. However, node 62 operated for 25 days in 2012 from DOY 270–295. During this time 180 events were recorded.

5.1. Data analysis

We first investigate the general relationship between the number of events per day and the meteorological conditions, and then look in more detail at the individual traces. The signal was similar on all three planes. Without multiple data sources and synchronisation it was impossible to use common detection to locate the ice quake in three dimensions. However it was possible to derive the dominant frequency of the events by fast Fourier transform analysis and carry-out event type classification. Using these two techniques we were able to interpret the styles of microseismicity recorded.

There was a generally positive relationship between events per day and glacier surface melt (Fig. 8a), and we can divide the results into three time periods based on geophone activity (Fig. 8a). High seismic activity (DOY 270–279), is associated with high and generally positive air temperatures at the base station. The day with the highest melt has

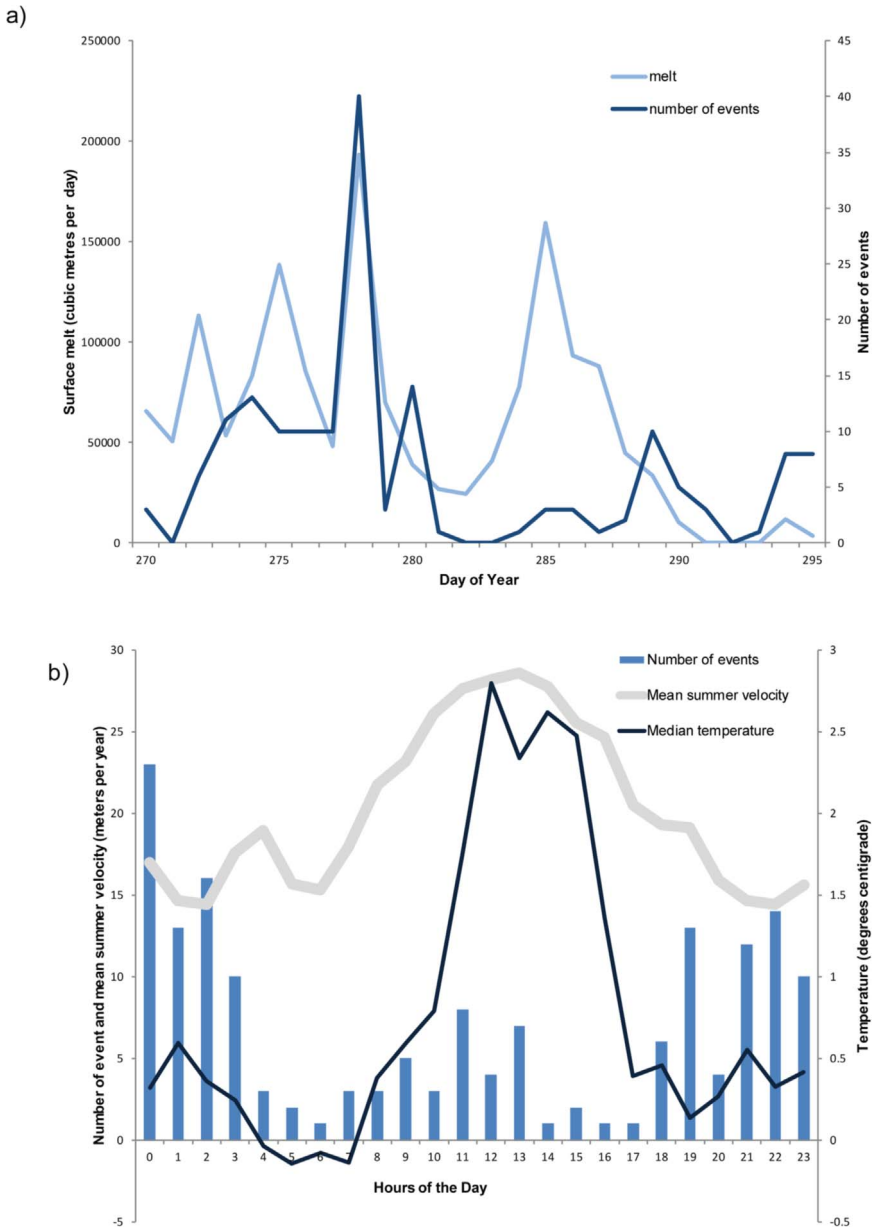

Fig. 8. a) Relationship between number of seismic events (dark line) and glacier surface melt (calculated from PDD) (light line); b) diurnal timing of seismic events.

the most events. This is followed by a period of low seismic activity (DOY 280–288), when air temperatures are lower and are below zero at night. Here the maximum events also occur on the day with the most melt. Finally, there is an intermediate seismic activity (DOY 289–295) during the winter when temperatures are almost always below zero, but on a few days' temperatures at the base station rose above zero (DOY289, 290, 294 and 295). Day 294 had the highest positive temperatures during this period and had the highest number of seismic events.

There was also a relationship between diurnal temperature patterns and events. At the site, the temperatures were lowest during the night (18:00–08:00) and warmest during the afternoon (12:00–16:00). The majority of seismic events occurred during the temperature rise and peak and during the night (Fig. 8b). The mean hourly summer ice velocity is also shown (from the available period DOY 218–269). Glacier velocities are highest during the temperature rise and peak and lowest during the night.

5.2. Classification of event types

Fast Fourier transform analysis was carried out on each trace, in order to find the dominant frequencies. In additional, each trace was manually analysed and classified. This enabled us to characterize the type of events into three forms (Table 1, Figs. 9 and 10):

- Type A – consisting of a low frequency wave (Fig. 9a). This typically has a dominant frequency of 14 Hz (with smaller peaks at 4 and 6 Hz).
- Type B – consisting of a distinct wave form which we interpret to reflect the P and S wave (Fig. 9b). This also has a dominant frequency of 4 Hz (and smaller peaks at 6 and 8 Hz).
- Type C – consisting of a cigar shaped envelope (Fig. 9c), with a dominant frequency of 6 Hz (and also 8–16 Hz)

Fig. 11 shows the diurnal occurrence of each event type during the three distinct time periods. During the high seismic activity period all three seismic types are found and 17% of events occurred during the

Table 1
Seismic event types.

	Type A	Type B	Type C
Onset	Emergent	Emergent	Impulsive
Amplitude	Monochromatic waveform	Monochromatic waveform, impulsive P and S wave and distinct coda	Episodic events, often forms cigar-shaped envelope
Spectra		Multiple pulses, lasting between 0.08 and 0.2 s with intervals 0.12 s	
Dominant frequency	14 Hz	4 Hz	6 Hz
Frequency range	3–40 Hz	3–22 Hz	3–38 Hz
% low frequency (3–18 Hz)	93%	95%	84%
% high frequency (19–40 Hz)	7%	6%	16%
Duration	> 1 s	Mean 0.18 s (s.d. 0.04 s)	Mean 0.13 s (s.d. 0.06 s)
Interpretation	Deformation	Sliding	Hydraulic

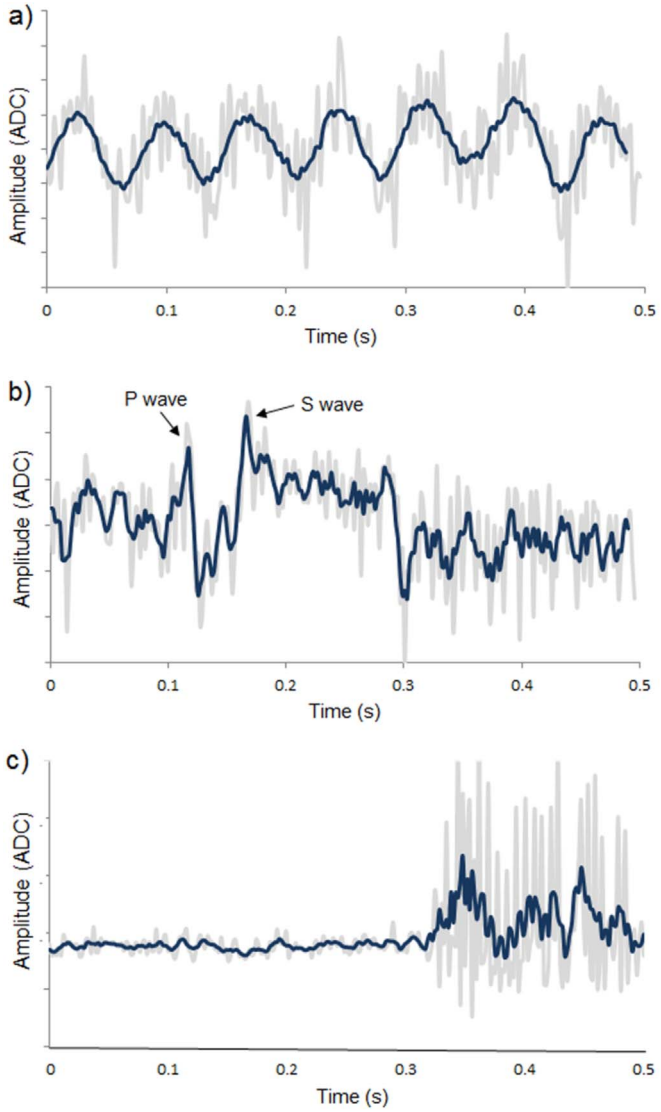

Fig. 9. Examples of different seismic event types (light line is unfiltered signal, dark line filtered to show the dominant frequency found from the FFT analysis): a) Type A, b) Type B, c) Type C.

temperature/velocity rise, 23% during the temperature/velocity maximum, and 60% after the temperature/velocity peak. Type A and C events occurred most during the temperature/velocity fall (73% and 100% respectively), whilst Type B occurred mostly during the temperature/velocity rise (33%).

During the low seismic activity period only Type A occurs, and 38% of events occurred during the temperature/velocity rise, 8% during the maximum, and 54% after the peak.

During the intermediate seismic activity (winter) period all three seismic styles are present, 76% of the events occurred when air temperatures were negative, and 80% of these were Type A events (16% Type C and 4% Type B) of which 86% occurred during the temperature/velocity decline.

5.3. Interpretation of the event types

It has been suggested that different microseismic sources can be identified by distinct wave forms, but that basal signals may be masked by other signals (in particular crevassing) (Pomeroy et al., 2013; Helmstetter et al., 2015). However, it has been shown that crevassing is typically characterized by high frequency (20–35 Hz) events (with short duration (< 1 s) impulsive onsets), whilst basal events are characterized by low frequency (6–15 Hz) events [46].

Our results show that 91% of the dominant frequencies were between 3–18 Hz, showing a prevalence of low frequency events. Combined with the evidence for basal events from the 2011 field trial, we conclude that our 3 event types reflect subglacial events.

Type A – These are the most common event type and occurred throughout the whole period, even when air temperatures were negative. They are most commonly found during the night. The characteristics of these signals (Table 1) were similar to those associated with subglacial sediment (till) deformation during stick-slip motion (Anandakrishnan and Bentley, 1993) especially during basal recoupling after a stick-slip event (West et al., 2010).

We have shown previously shown that at Skálafellsjökull subglacial deformation takes place throughout the year (Hart et al., 2015), and so suggest that Type A also reflects subglacial deformation. This process occurs as the glacier begins to accelerate in the morning, but this is more frequent when the glacier recouples with the bed as the glacier decelerates in the night.

A typical value for basal stick-slip is 1 mm in 0.01 s slip (Zoet et al., 2013). We measured 3 m a year till movement (with GPR) at Skálafellsjökull. If we assume this represents stick-slip this would require an average of 8.2 events per day. If we suppose our 3 seismic times represent summer, early spring/late autumn (when night temperatures are below zero) and winter respectively, we can calculate value of the annual average events per day. For Type A this would be 5 events per day (and for all events 7 events per day), which is remarkably similar to the predicted figure.

Type B – These are the second most common event, but have a far

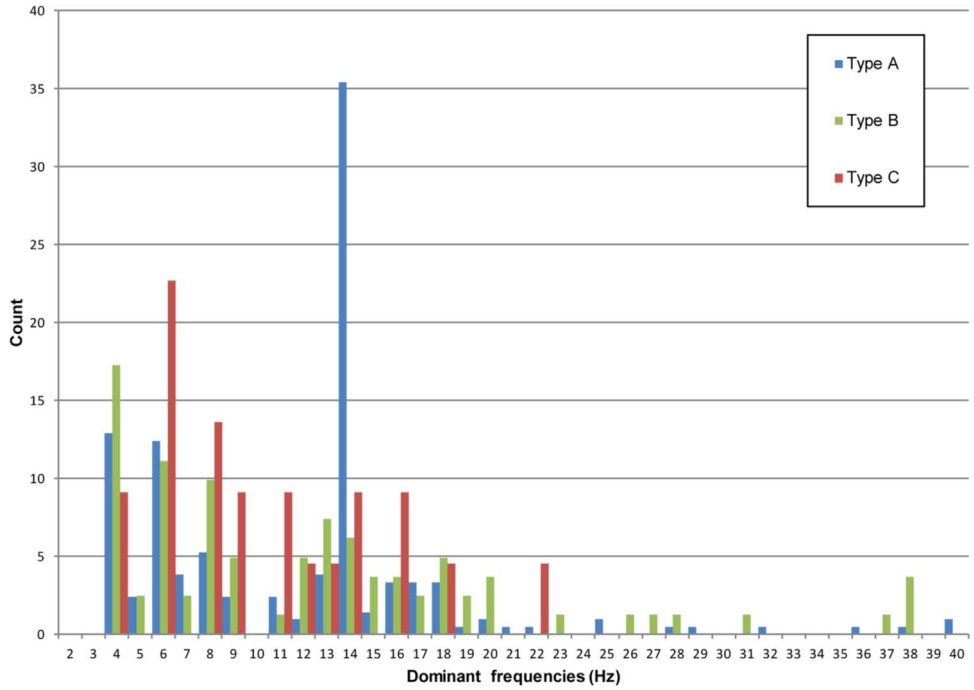

Fig. 10. Histogram of the top three dominant frequencies for each trace, separated into the three event types.

more restricted time range. During the high seismic activity period these events occurred either just before and/or during the temperature/velocity maxima. During the winter, these events only occurred during positive temperature days and these all occurred during the maxima in temperature/velocity.

This type has virtually identical wave forms with a distinct P and S waves with an average separation of 0.05 s (s.d. 0.02). The difference between the P and S waves gives an average depth of 180 m, which is within the range of the ice depth in the study area. We suggest the Type B events reflect a large main basal sliding event.

Type C – These are the least frequent of the event types. They only occur in the night (after the temperature/velocity maxima). Several researchers have suggested that low frequency signals with extended codas and weakly developed emergent onsets or no seismic phases (P and S waves), are typical of water sourced seismicity (Lawrence and Qamar, 1979; Stuart et al., 2005; West et al., 2010). Hydraulic events, possible disturbances of the water flow (associated with melting), that can generate a 'water hammer' effect in plumbing systems could cause the observed harmonic signal (Wolf and Davies, 1986; Kavanaugh and Clarke, 2001).

At Skálafellsjökull these events may reflect hydraulic disturbances associated with changing drainage pathways created as a result of the stick-slip events.

5.4. Evaluation of the system

The commercial system installed on the glacier surface in 2011 provided good evidence for basal events. However, this system required daily manual re-levelling and high levels of power supply. Thus this system could not be used for long-term automatic recordings. Due to noise from the glacier surface, rain, crevassing and melting, more processing was needed to interpret the data. The borehole system installed in 2012 automatically recorded the signals containing possible events. This system was less affected by noise and so only 180 events were recorded in 25 days which were shown to be non-random. The low power system design means it can be left running for long periods without solar generation. Improvements to the enclosures and software reliability would then allow long-term monitoring. The prototype radio network was successful and showed that the data volumes were not too high for a real deployment. Further development on the robustness of the system could allow more accurate isolation of the source of the basal signals (where multiple geophones are triggered simultaneously) and allow the investigation of the seasonal changes, particularly winter high discharge events (Young et al., 2015). An improved time synchronisation system is also needed which can operate over the radio network, this could be helped by including a GPS unit in each surface node.

6. Conclusion

This study has demonstrated the successful design and development of a borehole geophone as part of an environmental wireless sensor network. A field trial with commercial surface geophones served as a baseline and helped to determine the capture parameters. The design makes it feasible to obtain long term geophone event capture, with the data being transmitted back to a data server.

Our basal signals showed (as noted by other researchers, Smith, 2006) a predictable, periodic recurrence of signals which suggest similar source events, occurring regularly at a similar location from the release of accumulated stress. The results showed that there was a relationship between surface melt production and the number of microseismic events. These events occurred more frequently at specific times during the day. Three types of seismic events were identified. The most common was Type A, typified by an emergent, monochromatic waveform, which occurred mostly during the glacier velocity decrease, and was interpreted as till deformation. Secondly, Type B, an emergent monochromatic waveform, with impulsive P and S waves (with an average separation of 0.05 s), and only occurred during the glacier velocity rise and peak. This was interpreted as resulting from the main basal sliding event. Lastly, Type C, with a waveform comprising episodic events, often with a cigar-shaped envelope, occurring typically 11 h after the velocity peak. This is interpreted as reflecting hydraulic transience as the drainage system returns to 'normal'.

Future work to improve the reliability of the nodes would allow more locations to be sampled simultaneously to locate events. This would also require extra synchronisation, which could be implemented with small GPS units on each surface node. Testing the 173 MHz radio links to the surface could show that the backup cables are unnecessary

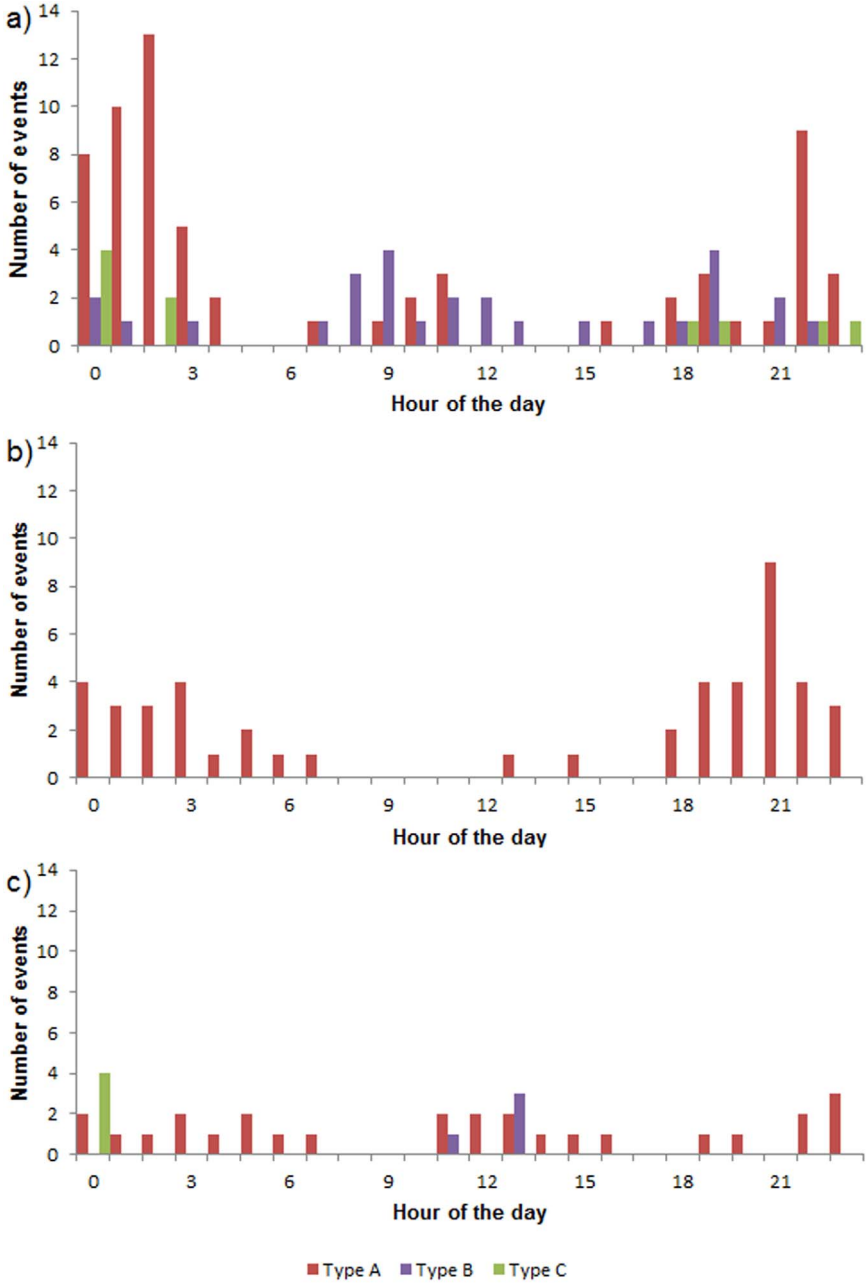

Fig. 11. Diurnal timings of the different seismic activity periods: a) high seismic activity (DOY 270-270), b) low seismic activity (DOY 280–288), c) intermediate seismic activity (DOY 289–295).

if extra batteries are enclosed in the nodes. The use of new techniques and technologies in this design has been shown to provide a breakthrough in the capabilities of long term continuous monitoring for geoscience.

Acknowledgements

The authors would like to thank the Glacsweb Iceland 2011 and 2012 teams for help with data collection and thanks to Laura Edwards, Matthew Burke and Andrew Turner for data processing, Dirk De Jager for PCB design and Mark Dover for Cartography, and Alex Brisbourne and Victoria Lane from SEIS UK for advice and field and data processing assistance. This research was funded by the ESPRC (Grant EP/C511050/1), the Leverhulme Trust (Grant number F/00 180/AK), National Geographic Society Science and Exploration Europe GEFNE45-12 and ARM. The NERC Geophysical Equipment Facility provided loans of the Seismology and GPR equipment.

References

Anandakrishnan, S., Bentley, C.R., 1993. Micro-earthquakes beneath Ice Streams B and C, West Antarctica: observations and implications. J. Glaciol. 39, 455–462.
Bahr, D.B., Rundle, J.B., 1996. Stick-slip statistical mechanics at the bed of a glacier. Geophys. Res. Lett. 23 (16), 2073–2076.
Braithwaite, R.J., 1985. Calculation of degree-days for glacier-climate research. Z. Gletsch. Glazialgeol. 20, 1–8.
Boulton, G.S., Jones, A.S., 1979. Stability of temperate ice caps and ice sheets resting on beds of deformable sediment. J. Glaciol. 24, 29–44.
Chong, C.Y., Kumar, S.P., 2003. Sensor networks: evolution, opportunities, and challenges. Proc. IEEE 91 (8), 1247–1256.
Deichmann, N., Ansorge, J., Scherbaum, F., Aschwanden, A., Bernardi, F., Gudmundsson, G.H., 2000. Evidence for deep icequakes in an Alpine glacier. Ann. Glaciol. 31 (1), 85–90.
Delin, K.A., Jackson, S.P., Johnson, D.W., Burleigh, S.C., Woodrow, R.R.J., Mcauley, M., Dohm, J.M., Ip, F., Ferré, T.P.A., Rucker, D.F., Baker, V.R., 2005. Environmental studies with the Sensor web: principles and practice. Sensors 5, 103–117.

Duval, P., 1977. The role of water content on the creep rate of polycrystalline ice. IAHS 118, 29–33.
Fischer, U.H., Clarke, G.K.C., 1997. Stick-slip sliding behaviour at the base of a glacier. Ann. Glaciol. 24, 390–396.
Gehrke, J., Liu, L., 2006. Sensor-network applications. IEEE Internet Comput. 10, 16–17.
Hart, J.K., Martinez, K., 2006. Environmental Sensor Networks: a revolution in the earth system science? Earth-Sci. Rev. 78 (3), 177–191.
Hart, J., Martinez, K., Edwards, L., 2011. Investigating glacier stick-slip motion using a wireless Sensor Network. Report for NERC GEF. p. 10.
Hart, J.K., Martinez, K., Ong, R., Riddoch, A., Rose, K.C., Padhy, P., 2006. A wireless multi-sensor subglacial probe: design and preliminary results. J. Glaciol. 52 (178), 389–397.
Hart, J.K., Rose, K.C., Clayton, A.I., Martinez, K., 2015. Englacial and subglacial water flow at Skálafellsjökull, Iceland derived from ground penetrating radar, in situ Glacsweb probe and borehole water level measurements. Earth Surf. Process. Landf. 40 (15), 2071–2083.
Helmstetter, A., Nicolas, B., Comon, P., Gay, M., 2015. Basal icequakes recorded beneath an Alpine glacier (Glacier d'Argentière, Mont Blanc, France): evidence for stick-slip motion? J. Geophys. Res. Earth Surf. 120, 379–401.
Hock, R., 2003. Temperature index temperature modelling in mountain areas. J. Hydrol. 282, 104–115.
Hasler, A., Talzi, I., Beutel, J., Tschudin, C., Gruber, S., 2008. Wireless sensor networks in permafrost research: Concept, requirements, implementation, and challenges. In: Proceedings of the 9th International Conference on Permafrost, Fairbanks, US, 669–674.
Huang, Y., Martinez, J.-F., Sendra, J., López, L., 2015. Resilient wireless sensor networks using topology control: a review. Sensors 15, 24735–24770.
Iken, A., Röthlisberger, H., Flotron, A., Haeberli, W., 1983. The uplift of Unteraargletscher at the beginning of the melt season — a consequence of water storage at the bed? J. Glaciol. 29, 28–47.
Johannesson, T., Sigurdsson, O., Laumann, T., Kennett, M., 1995. Degree-day glacier mass-balance modelling with applications to glaciers in Iceland, Norway and Greenland. J. Glaciol. 41 (138), 345–358.
Kavanaugh, J.L., Clarke, G.K.C., 2001. Abrupt glacier motion and reorganization of basal shear stress following the establishment of a connected drainage system. J. Glaciol. 47, 472–480.
Lawrence, W.S.T., Qamar, A., 1979. Hydraulic transients: a seismic source in volcanoes and glaciers. Science 203, 654–656.
Martinez, K., Basford, P., 2011. Robust wireless sensor network performance analysis. IEEE Sens. Limerick.
Martinez, K., Hart, J.K., Ong, R., 2004. Environmental Sensor Networks. IEEE Comput. 37 (8), 50–56.
Martinez, K., Hart, J.K., Ong, R., 2009. Deploying a Wireless Sensor Network in Iceland, lecture notes in computer science. Proceedings of the Geosensor Networks. 5659, 131–137.
Martinez, K., Basford, P.J., De Jager, D., Hart, J.K., 2012. A wireless sensor network system deployment for detecting stick slip motion in glaciers. In, IET International conference on Wireless Sensor Systems, London, GB, 18–19 Jun, p. 3, 14-16.
Metaxian, J.-P., Araujo, S., Mora, M., Lesage, P., 2003. Seismicity related to the glacier of Cotopaxi Volcano Equador. Geophys. Res. Lett. 30 (9), 1483.
Neave, K.G., Savage, J.C., 1970. Icequakes on the Athabasca Glacier. J. Geophys. Res. 75 (8), 1351–1362.
Oliveira, L.M.L., Rodrigues, J.J.P.C., 2011. Wireless Sensor Networks: a survey on environmental monitoring. J. Commun. 6, 143–151.
O'Neel, S., Pfeffer, W.T., 2007. Source mechanics for monochromatic icequakes produced during iceberg calving at Columbia Glacier, AK. Geophys. Res. Lett. 34 (22).
Pomeroy, J., Brisbourne, A., Evans, J., Graham, D., 2013. The search for seismic signatures of movement at the glacier bed in a polythermal valley glacier. Ann. Glaciol. 54 (64), 149–156.
Qamar, A., 1988. Calving icebergs: a source of low-frequency seismic signals from Columbia Glacier, Alaska. J. Geophys. Res. 93 (B6), 6615–6623.
Rothlisberger, H., 1972. Seismic exploration in cold regions. Cold Reg. Sci. Monogr. II-A 2a, Hanover, CRREL, 139.
Sigurðsson, O., 1998. Glacier variations in Iceland 1930–1995. Jökull 45, 3–25.
Smith, A.M., 2006. Microearthquakes and subglacial conditions. Geophys. Res. Lett. 33 (24).
Song, W.-Z., Huang, R., Xu, M., Ma, A., Shirazi, B., LaHusen, R., 2009. Air-dropped sensor network for real-time high-fidelity volcano monitoring. In: Proceedings of the 7th International Conference on Mobile systems, applications, and services, Wroclaw, Poland.
Tsai, V.C., Ekstrom, G., 2007. Analysis of glacial earthquakes. J. Geophys. Res. 112, F03014.
Stuart, G., Murray, T., Brisbourne, A., Styles, P., Toon, S., 2005. Seismic emissions from a surging glacier: bakaninbreen. Svalbard, Ann. Glaciol. 42, 151–157.
Szewczyk, R., Osterweil, E., Polastre, J., Hamilton, M., Mainwaring, A., Estrin, D., 2004. Habitat monitoring with sensor networks. Commun. ACM 47 (6), 34–40.
Walter, F., Deichmann, N., Funk, M., 2008. Basal icequakes during changing subglacial water pressures beneath Gornergletscher, Switzerland. J. Glaciol. 54 (186), 511–521.
Weaver, C.S., Malone, S.D., 1979. Seismic evidence for discrete glacier motion at the rock-ice interface. J. Glaciol. 23 (89).
Weertman, J., 1957. On the sliding of glaciers. J. Glaciol. 3, 33–38.
Werner-Allen, G., Johnson, J., Ruiz, M., Lees, J.M., Welsh, M., 2005. Monitoring volcanic eruptions with a wireless sensor network. In: Proceedings of the European Workshop on Sensor Networks (EWSN'05), #1568945184.
West, M.E., Larsen, C.F., Truffer, M., O'Neel, S., LeBlanc, L., 2010. Glacier microseismicity. Geology 38, 319–322.
Wiens, D.A., Anandakrishnan, S., Winberry, J.P., King, M.A., 2008. Simultaneous teleseismic and geodetic observations of the stick–slip motion of an Antarctic ice stream. Nature 453 (7196), 770–774.
Wolf, L.W., Davies, J.N., 1986. Glacier-generated earthquakes from Prince William Sound, Alaska. Bull. Seismol. Soc. Am. 76, 367–379.
Xu, G., Shen, W., Wang, X., 2014. Applications of wireless sensor networks in marine environment monitoring: A survey. Sensors, 14, 16932–16952.
Young, D.S., Hart, J.K., Martinez, K., 2015. Image analysis techniques to estimate river discharge using time-lapse cameras in remote locations. Comput. Geosci. 76, 1–10.
Zoet, L.K., Alley, R.B., Anandakrishnan, S., Christianson, K., 2013. Accelerated subglacial erosion in response to stick-slip motion. Geology 41, 159–162.